X-ray atomic absorption of cesium and xenon in the *L*-edge region

A. Kodre,[1,2] J. Padežnik Gomilšek,[3] I. Arčon,[4,2] and G. Aquilanti[5]
[1]*Faculty of Mathematics and Physics, University of Ljubljana, Jadranska 19, SI-1000 Ljubljana, Slovenia*
[2]*J. Stefan Institute, Jamova 39, SI-1000 Ljubljana, Slovenia*
[3]*Faculty of Mechanical Engineering, University of Maribor, Smetanova 17, SI-2000 Maribor, Slovenia*
[4]*University of Nova Gorica, Vipavska 13, SI-5000 Nova Gorica, Slovenia*
[5]*Sincrotrone Trieste S.C.p.A s.s. 14, km 163.5, I-34149 Basovizza, Trieste, Italy*
(Received 18 July 2010; published 26 August 2010)

X-ray absorption of atomic cesium is measured in the *L*-edge region, using a beryllium-window cell for cesium vapor. For comparison, absorption in Xe gas in the same energy region is remeasured with improved signal-to-noise ratio. By combining deconvolution and modeling, the edge profiles are studied to determine the threshold energies and the shape of the edge apex with exponential slope of the high-energy flank. In both elements, multielectron excitations show the same basic ordering in compact groups, largely independent of the core-hole subshell, following the energy sequence of coexcited valence and subvalence orbitals. The main effect of $6s$ electron in Cs, apart from $2(s,p)6s$ excitation, is the enhancement of single- as well as some multielectron resonant channels. The spectra of both elements show the "polarization effect": a convex basic curvature of the L_2 and L_3 segments, a concave L_1 segment. Previously, Kutzner demonstrated a convincing theoretical explanation of the effect on Xe in a relativistic random-phase approximation with relaxation involving overlap integrals with continuum [Rad. Phys. Chem. **70**, 95 (2004)].

DOI: 10.1103/PhysRevA.82.022513 PACS number(s): 32.30.Rj, 32.80.Aa

I. INTRODUCTION

In the x-ray absorption of pure elements in the monatomic state, the interaction between the photon field and the atomic quantum system is directly measured. Within the prevailing process of photoelectric absorption, small contributions of collective excitations, real and virtual, of the atom can be discerned in the vicinity of major absorption edges. Complex multiple-excitation atomic states can be studied in this way [1].

With the exception of noble gases, which have been exhaustively investigated, the monatomic state of an element is difficult to prepare. Although most metals in the state of vapor are almost completely monatomic, the main problem of an experiment is to keep the hot vapor of appropriate density, only an order of magnitude smaller than that of ambient air, as a stable absorption sample. So far, the absorption in the extended *K*-edge regions of the relatively volatile metals Rb, K, Cs, Zn, and Cd [1–5] has been measured in experiments with vapor temperatures below 1000°C. *K*-edge profiles have been determined for the less volatile metals Ca, Cr, Mn, and Cu [6]. A high-temperature experiment was also devised for preparation of monatomic iodine by exploiting the dissociation of the molecular vapor [7].

The coverage of *L*-edge regions is scarce: Standard x-ray absorption spectroscopy has only been used in several absorption studies on xenon [8,9] and mercury [10]. The conflicting demands of cell window material for a volatile-metal experiment (heat and corrosion resistance, vacuum tightness, and x-ray transparency) are considerably harder to reconcile in the low-energy region of *L* edges.

In the cesium experiment, we used the type of cell developed for the *K*-edge spectroscopy of potassium vapor [11]. The relative absorption cross section was measured within a 1300-eV-wide *L*-edge region. In the identification of reaction channels in the edge profiles and in the small spectral features of multielectron excitations the comparison with the absorption data of the neighbor element xenon was helpful. For the purpose, Xe *L*-edge absorption was remeasured with improved resolution and signal-to-noise ratio.

The structure of the *L*-edge profiles of Cs and Xe is discussed, providing a check and calibration points for theoretical values and for x-ray metrology. A combined approach of deconvolution and modeling is adopted. In the overview of multielectron photoexcitations (MPE), the main problem is recognized in the concept of the "spectrum baseline" upon which the MPE are superposed. The concept, useful in identification of *K*-edge MPE, breaks down for $2p$ edges. Recent advances in theory offer a good guideline for a new paradigm.

II. EXPERIMENT

The absorption cell for cesium vapor is a 10-cm-long stainless-steel tube with inner diameter of 6 mm, to which the window flanges are welded. The beryllium windows are brazed to the flanges with silver foil. Before assembly, all parts are baked out in a hydrogen atmosphere to remove the adsorbed water and the surface oxide layer. The cesium charge is introduced through a side tube in snippets of a hypodermic needle. The cesium container is warmed up slightly, and the melted metal is drawn into the needle with a syringe. After a short dip in liquid nitrogen the metal is frozen to immobility and the needle is safely cut into pieces of appropriate length. The cell is evacuated and the side tube is closed first by cold beating and finally by welding.

The absorption experiment was performed at the beamline C of Hasylab, DESY, equipped with a Si 111 two-crystal monochromator with a resolution of 0.6 eV. Higher-order harmonics were effectively eliminated by detuning of the monochromator crystals to 60% of the rocking curve maximum, using beam-stabilization feedback control. The gas fillings of the three ionization detectors on the beamline were

optimized for the energy range 4700 to 6100 eV: 400 mbar N_2, 160 mbar Ar, and 250 mbar Ar. The cell was inserted into a tubular oven with 3-μm-thick Al windows and a He atmosphere and was aligned on the beam. The absorption scan over the entire energy interval was taken on the cold cell to determine the attenuation along the beam path, that is, in the air and He gas in the oven, as well as in the Be and Al windows. The oven was programmed to heat up slowly to 700°C and the absorption in the Cs vapor was monitored until saturation was reached, indicating the complete evaporation of the metal.

With saturated and stable Cs vapor density, five consecutive absorption scans with an integration time of 1 s/step were collected to improve the signal-to-noise ratio and to check the stability and reproducibility of the detection system. Energy steps of 0.25 eV were used within 270-eV-wide edge regions, and 0.5 eV steps were used elsewhere.

For the precise calibration of the energy scale, the absorption in thin foils of titanium, vanadium, and chromium was measured between the posterior pair of ionization detectors, simultaneously with Cs absorption.

The *L*-edge absorption of xenon was remeasured at the XAFS beamline of the ELETTRA synchrotron at Trieste, exploiting its improved optics and stability [13]. Xenon was contained in a 4-cm-long absorption cell with kapton foil windows at a pressure of 160 mbar. A Si 111 monochromator with a resolution of 0.6 eV and detuning of 40% was used. The beam intensity was measured with ionization detectors filled with 200 mbar N_2, 1100 mbar N_2, and 140 mbar Ar + 860 mbar N_2, respectively, and with He up to a total pressure of 2000 mbar. The absorption spectra were measured within the energy interval interval of 4500 to 6500 eV. The entire interedge region (4750–5750 eV) was scanned with energy steps of 0.25 eV, and the end segments were scanned with 1-eV steps. Five scans with integration time of 2 s/step were collected and superposed to improve the counting statistics. A simultaneous absorption measurement on the Ti foil provided a precise energy calibration.

III. RESULTS

The quality of the measured spectra of Cs and Xe is close to the present limit of absorption spectroscopy. The respective relative noise levels, achieved by superposition of scans, are 5×10^{-4} and 5×10^{-5}. The resolution of the monochromators makes the experimental width (FWHM) only about 20% of the lifetime width, leading to an almost imperceptible widening of the spectral features. Indeed, the comparison of the Xe spectrum with earlier data shows a distinctly sharper spectrum detail.

As can be seen in Fig. 1, the L_1 and L_2-L_3 edge profiles differ in the strength of the "white line" and in the apex of the edge itself. Another major dissimilarity is the difference in the slopes and curvatures of the smooth cross-section segments between the respective edges.

In the analysis of the data which involves the identification of the reaction channels, the comparison with neighbor elements, or, for valence coexcitations, the comparison with congener elements, may offer some clue. With the improved quality of the data obtained on modern devices, two quantitative techniques have been developed. In the modeling

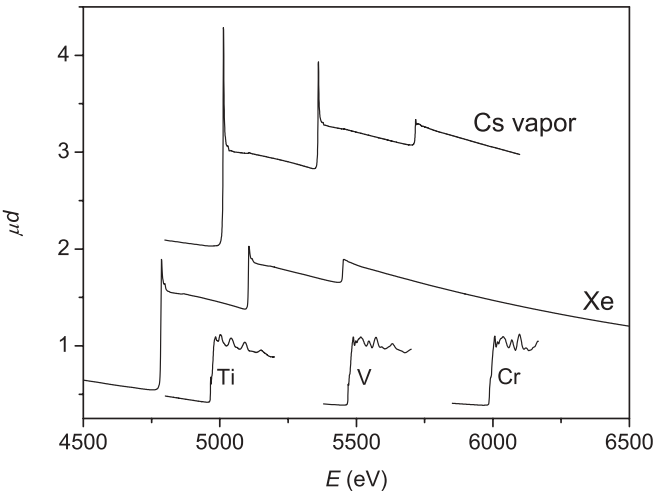

FIG. 1. A panoramic view of the Cs and Xe atomic absorption in the *L*-edge region, together with the *K*-edge scans of metals Ti (4964.6 eV), V (5463.8 eV), and Cr (5989.0 eV) [12]. Cs and Xe data are normalized to the same L_3 edge jump and displaced vertically for clearer view.

approach, a segment of a spectrum is approximated by an ansatz of fundamental spectral shapes such as Lorentzian peaks and arctangent edges. Free parameters of the ansatz (e.g., the amplitudes of the ansatz functions, the threshold energies, and the width parameters) are determined by a least-square fitting procedure [1,2].

Another approach, critically dependent on the quality of data, is deconvolution. Filipponi [14] has shown that the Lorentzian shape of spectral features can be converted into corresponding Gaussian shapes with some gain in the effective width. However, it follows from information theory that the gain is compensated by some loss of information, in this case in the increase of the noise level. Thus, experimental data with a very good signal-to-noise ratio can be sharpened to some extent [1,3]. The technique is a pure geometrical model-free transformation of the data. It works best on large spectral features such as absorption-edge profiles, since they best withstand the increased noise level, while the resolution gain in the smaller features tends to be drowned by the noise. Very good results can be obtained in separating blended large features and in exposing small features from underneath broad Lorentzian line tails.

A. Edge profiles

In addition to the dominant channel of the core ionization $[2s,p]$, the edge profile also hides the resonant excitations $[2s]np$ or $[2p]nd,s$ of the Rydberg series and possibly some valence coexcitations. A comprehensive modeling of the edge profile with a large number of highly correlated parameters in the ansatz can only be applied with extensive borrowing of theoretical or tabulated data for excitation energies and widths, as in the decomposition of noble-gas edge profiles by Breinig *et al.* [15]. A practical solution of the problem has been demonstrated by Teodorescu *et al.* [16]: Only a few leading resonances of the Rydberg series, often a single one, can be resolved in majority of elements, while the unresolved

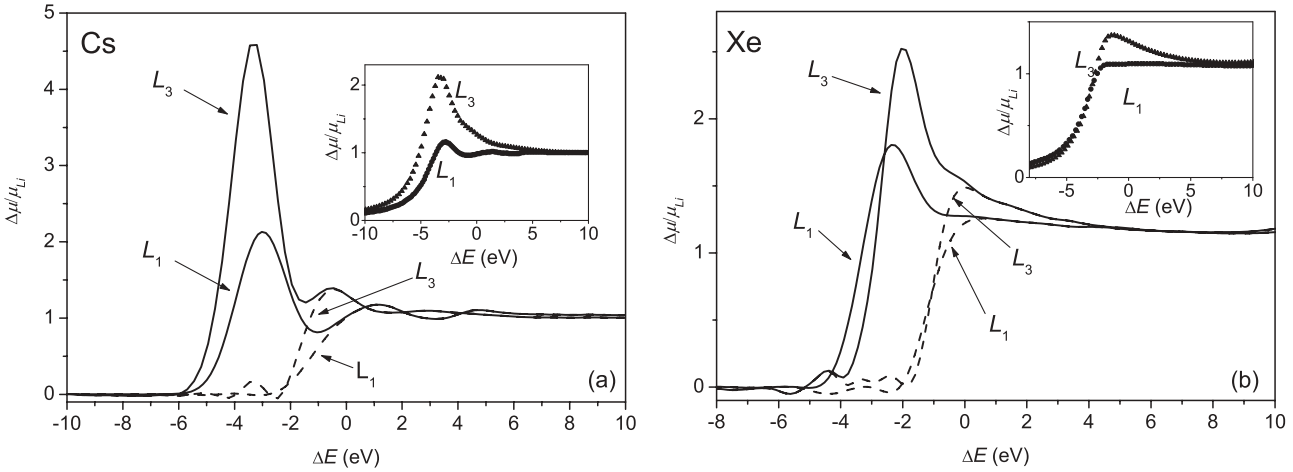

FIG. 2. The deconvoluted L_1 and L_3 edge profiles (solid line) of Cs (a) and Xe (b) in the energy scale relative to the respective continuum threshold. The apparent edges are shown after removal (dashed line) of the pre-edge resonance converted into a Gaussian. Natural profiles are shown in the inserts.

resonances blend with the continuum contribution, producing an effective absorption edge shifted to lower energy.

Another effect, modifying the edge region, is the post-collision interaction (PCI) [17,18]. No simple analytical form of its contribution has been derived from theory. In K edges of a number of elements, a heuristic approximation in the form of a simple exponential has been successfully used in models [1], with the range of the exponential roughly proportional to the edge energy.

In the case of L edges the problem seems even more complex. The overview of the normalized edge regions (inserts in Fig. 2) shows that the PCI contribution depends on the angular momentum of the photoelectron. The exponential ansatz with ~35-eV range seems appropriate for the L_1 edges of Xe and Cs. In L_2 and L_3 edges the range is less than 6 eV.

Although the PCI contribution is plainly visible and its decay range well defined, its onset at the threshold is not known. The lack of an exact analytical form of the ionization edge with PCI is particularly troublesome in combination with strong pre-edge resonance channels. The distribution of the intensities among the channels in modeling of the experimental data is strongly susceptible to the details of the model functions.

Consequently, the model-free deconvolution is used as a first step. By decreasing the width of the channel components, the overlap of the leading resonance with the edge is reduced to its high-energy flank, so that the low-energy flank can be modeled by a Gaussian ansatz. With that, the resonant contribution is removed and the edge is exposed.

The deconvoluted edges and their components in Cs and Xe are shown in Fig. 2. The leading resonance is well separated from the apparent edge so that both energies can be reliably determined. In the Xe L_3 decomposition, a tiny peak at the low-energy flank of the leading resonance can be discerned. It is the fingerprint of the $[2p]6s$ resonance, 1.6 eV below the $[2p]5d$ line by the Hartree-Fock (HF) [19] estimate. In Cs, the resonance is only 0.9 eV below the $[2p]5d$ and remains hidden.

Since the edge energy is modified by the contributions of the unresolved resonances of the Rydberg series, the ionization threshold energy, to be compared with theory, is determined from the leading resonance (Table I) using a HF estimate of the energy of the first Rydberg member relative to the continuum. The energies of the apparent edges are, as expected, close to the energies of the respective second members of the Rydberg series.

TABLE I. Ionization thresholds. Energies of the deconvoluted resonance and edge, in combination with the energies of the first two resonances of the Rydberg series, relative to the series limit, from the HF model. ΔE_2 provides a test of the Teodorescu hypothesis, and ΔE_1 is used to determine the ionization threshold from the energy of the resonance. In the second column of the data, the relative strength of the resonance is given. Uncertainties of the last digit are given in parentheses.

	Experiment			HF calculation ionization threshold			
	Resonance (eV)	Relative strength	Edge (eV)	ΔE_1 (eV)	ΔE_2 (eV)	This work (eV)	Theory[a] (eV)
Xe L_1	5450.3	1.4(3)	5451.4	−2.3	−1.2	5452.6(10)	5453.7(13)
Xe L_2	5104.7	1.7(3)	5105.7	−1.8	−1.0	5106.5(10)	5108.10(37)
Xe L_3	4784.3	1.5(3)	4785.2	−1.8	−1.0	4786.1(10)	4788.22(32)
Cs L_1	5717.3	1.9(3)	5719.3	−3.0	−1.3	5720.3(10)	5721.4(10)
Cs L_2	5361.4	3.9(3)	5362.9	−3.3	−1.2	5364.7(10)	5367.05(39)
Cs L_3	5014.0	3.7(3)	5015.6	−3.3	−1.2	5017.3(10)	5019.87(32)

[a]Reference [12].

The resulting energies of the ionization thresholds are compared to the recent NIST (National Institute of Standards and Technology) compilation of theoretical values [12]. The discrepancies are mostly outside of the combined uncertainty intervals. The estimated experimental error of 1 eV stems mostly from external sources, since the uncertainties of the fitting procedure remain below 0.2 eV. The HF values of ΔE_1 may contribute a comparable amount. The largest uncertainty is introduced by the calibration of the energy scale. Although the inflection points in edge profiles of the metal absorbers (Ti, V, and Cr) on the monochromator energy scale can be determined within 0.2 eV, the tabulation by the same source (NIST) introduces ~0.5 eV uncertainty, even within either of two categories of data (experimental-direct or experimental-combined), while the divergence of the two can be considerably larger. In this work experimental-direct data are used.

Since the deconvolution procedure conserves the integral intensity of spectrum components, the intensity of the resonance is estimated by a product of its width and amplitude, normalized to the unit edge jump. The values in the second data column of the table show that the L_2 and L_3 resonances in both elements are, as expected, equally strong within the error margin. In Xe, the L_1 resonance is only slightly weaker, contrary to the first impression from the original spectra. It is just that the energy step between the first two Rydberg members is larger. In Cs, the excitation channel is generally stronger, with particularly strong $L_{2,3}$ resonances. A similar effect has been observed in K edges of Ar and K [2], attributed to the increased effective nuclear charge of the excited $4p$ orbital in potassium due to weak screening by the $4s$ electron [20]. The analogous explanation can be invoked in the present case: Due to the weak screening by $6s$ electron of Cs the effective nuclear charge felt by the electron in the excited $6p$ orbital is greater than in Xe, lowering the energy of the excited state and increasing the $2s \rightarrow 6p$ matrix element. The effect is stronger yet for the $[2p]5d$ state, since the screening of the $5d$ orbital by the 6s electron is still weaker.

B. Multielectron excitations

The angular momentum of the core vacancy affects the shape of the spectrum above the edge: The L_3 and L_2 segments exhibit a convex shape, in opposition to the prevailing concave curvature of the absorption spectra. As discussed in the previous section, $2s$ and $2p$ edges differ also in the short segment of steeper negative slope (PCI) immediately above the edge.

To expose the small MPE features above the edge, the standard procedure in analysis of K-edge spectra has been used [1]. It involves the removal of the asymptotic Victoreen trend $AE^{-\gamma}$ of the cross section, determined in the extreme high-energy part of the measured spectrum, and of the exponential PCI ansatz, determined from the slope of the cross section between the major MPE groups. Analogously, in the L data of Cs and Xe, we determine the Victoreen trend in the far high-energy data segment above the L_1 edge and assume its exponent γ constant for the "baseline" of the entire L absorption spectrum, with just the coefficient A adapted for each interedge segment. This is in opposition to the approach of Zhang *et al.* [8], where the local slope below an edge was assumed to continue as a baseline to the region above the edge.

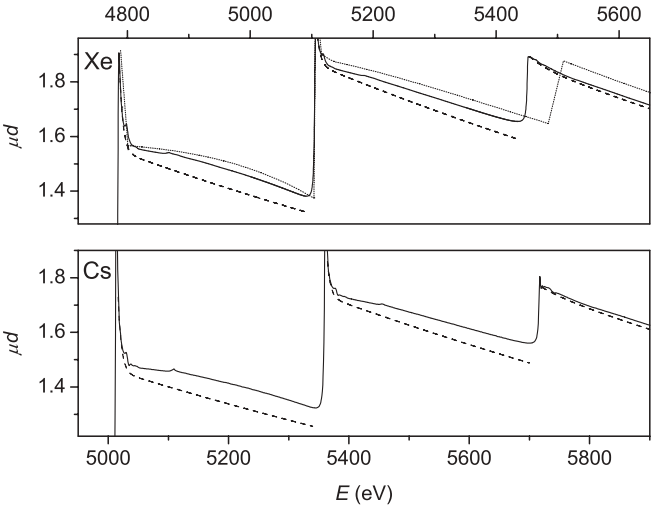

FIG. 3. The compound absorption spectrum (solid line) of Cs (below) and Xe (above) together with the smooth tentative baseline segments (dashed line)—the sum of Victoreen and PCI contributions. In the Xe plot, Kutzner's RRPARC calculation (dotted line), digitized with permission from Ref. [22], is also shown. Note that experimental values for the L_2- and L_3-edge energies are used in the calculation, along with the Hartree-Fock value for L_1.

After the removal of the local Victoreen trend and the PCI exponential, determined from the high-energy slope of each edge resonance, as shown in Fig. 3, the candidate MPE groups appear as shown in Fig. 4. Both L_1 sequences are similar to the sequences above K edges in general: a stepwise increase (with exception of resonances) of the cross section at the thresholds of individual excitation channels. The L_2 and L_3 sequences are not steplike and L_3 not strictly increasing. Apparently, an additional contribution is required to account for the general convex shape (i.e., the increase in the first half of a segment between the consecutive edges, and a decrease in the second half). To model the increase, an unusually large shake-off

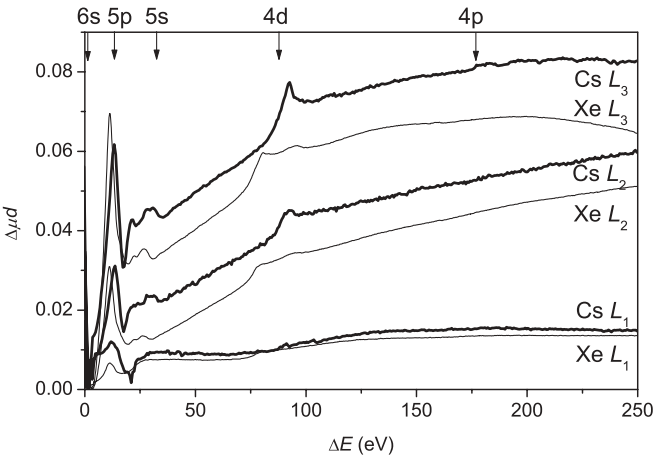

FIG. 4. The MPE subshell remainders after removal of the tentative baseline, in the common energy scale with origin at the respective edge. Comparison of the Cs and Xe data on a common absorption scale is achieved through renormalization with the NIST XCOM [23] tables. The main MPE groups are indicated with markers at SCF energies [24].

contribution from the subvalence orbitals, however unlikely, might be invoked; for the decrease, on the other hand, none of the standard MPE ansatz functions could be used.

The specific shape of L_2 and L_3 absorption has been discussed earlier. Jitschin and Stotzel [21] introduced a specific "polarization term" in the independent-particle Hamiltonian to account for the dipolar character of a p core vacancy. Zhang *et al.* [8] described the effect locally, drawing attention to the negative change of slope at the $2p4d$ group of the MPE, yet the results of their Δ self-consistent-field (ΔSCF) calculation gave the baseline curvature of the wrong sign. An *ab initio* calculation of the Xe photoabsorption cross section by Kutzner [22] gives L-edge baseline shapes closely similar to the experimental data. The result of his relativistic random-phase approximation (RRPA) calculation is similar to Zhang's, the RRPAR (RRPA with relaxation) introduces the right curvature, and RRPARC (RRPAR involving overlap integrals with continuum final-state orbitals) brings the result into a fair accord with experiment.

Kutzner's result shows that the concept of MPE and baseline superposition cannot be applied, since the terms in the modern perturbation calculations cannot be reduced to the simple single-electron–multielectron logic. The crucial terms of RRPARC may include the contribution of shake channels as well. The complexity of the problem is indicated also by the fact that the baseline curvatures of L_3 and L_2 edges are not of the same shape, just proportional by a factor close to 2. Such proportionality can be established for the edge profiles, as well as for the MPE features, which, in the L_2 and L_3 segments brought to a common relative energy scale and normalized to the same edge jump, subtract with almost no sharp features in the remainder. The RRPARC cross section, as Kutzner shows, is j dependent, with the L_3:L_2 ratio only tending to the value of 2 at the high-energy end of the segments.

As in the analysis of the edge profile, the high quality of the measured spectra at the moderate linewidth reveals a wealth of detail also in the domain of multielectron excitations. The quality can be best judged in a comparison of Cs L_1 data to the deconvoluted K-edge data [3] (Fig. 5). From the featureless K-edge absorption spectrum, a few wide humps

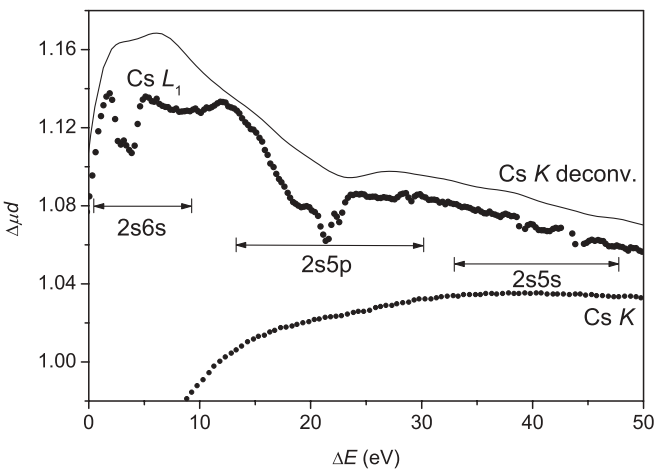

FIG. 5. A demonstration of the high resolution of Cs L_1-edge absorption spectrum in comparison with the K-edge spectrum, as measured and after deconvolution.

and valleys pertaining to the entire MPE groups are revealed after the deconvolution, while in L_1 data, several individual MPE channels are distinguished within each group.

In the overview of subshell MPE for Cs and Xe in Fig. 4, five main MPE groups (coexcitation of $6s$, $5p$, $5s$, $4d$, and $4p$ electrons) are indicated by the relative Dirac-Fock [24] configuration interaction (CI) energy of the lowermost channel in Cs, following the sequence of successive valence and subvalence shells. The separation of the groups is slightly smaller in Xe with the lower atomic number. For each element, however, the sequence of the relative MPE energies is almost independent of the subshell edge. The same energies, within experimental error, have also been observed in the K-edge spectra of Cs and Xe [3]. For Xe, the experimental energies for the main MPE, together with some excitation probabilities, have already been determined in an earlier study [9].

Even before a detailed quantitative analysis of the MPE features, some general observations can be given by a comparison of the L-edge and K-edge Cs and Xe spectra (Fig. 6).

The angular momentum of the core vacancy affects the shape of MPE features through the relative amplitudes of the constituting reaction channels. In Cs, the coexcitation of the outer, weakly bound $6s$ electron appears in the vicinity of the main edge: The $[2p6s]5d7s$ resonance lies below the $2p$ ionization threshold and is hidden in the apparent L_2 and L_3 edges while the $[2s6s]6p7s$ resonance is well resolved $\sim$1 eV above the L_1 edge. Moreover, the subsequent Rydberg member $[2s6s]7s7p$ and the shake-up edge $[2s6s]7s$ can be recognized in Fig. 5 at $\sim$3 and $\sim$5 eV, respectively.

The full profile of the resonance $[2s5p]6p^2$ in Cs at $\sim$12 eV cannot be reliably determined for the vicinity of the $2s6s$ shake, yet it seems to follow the general trend in alkali-metal–noble-gas pairs: The resonance in Cs is smaller and wider than in Xe, where the double transition to the $[2s5p]6p^2$ state coincides with the single-electron transition $2s \rightarrow 5p$ from the $[5p]^2 5d^2$ CI admixture of the ground state. The $[2s5p]$ shake channels blend with $5s$ coexcitation, resulting in extremely complex structure in Cs. The corresponding spectral interval in $2p$ edges is dominated by the leading resonance in both elements. The resonance and subsequent MPE features are, as already mentioned, identical in L_2 and L_3 when scaled to the corresponding edge jump, and, generally, stronger than L_1 features.

In the $4d$ group, the relative strengths of the resonant and shake channels show considerable variation. In L_1 spectra, the small $2s4d$ edge is the prevailing feature. In L_2-L_3 spectra, Xe exhibits a moderate resonance and Cs a prominent one. It has been speculated that nd coexcitations contribute a small replica of the main edge to the absorption spectrum. The finding is supported by a number of L absorption spectra of compounds of elements from iodine well into the lanthanide group, where the resonance of the $4d$ coexcitation follows the strength of the white line at the respective edge [25–27]. If the d orbitals involved in the monopolar coexcitation do not participate in the chemical bond of the atom, the constant $nd \rightarrow n'd$ part of the matrix element can be factorized out, and the probability of the nd coexcitation channels is proportional to respective single-electron channels of the main edge. For the pure atomic absorption, the speculation could so far be tested only in the

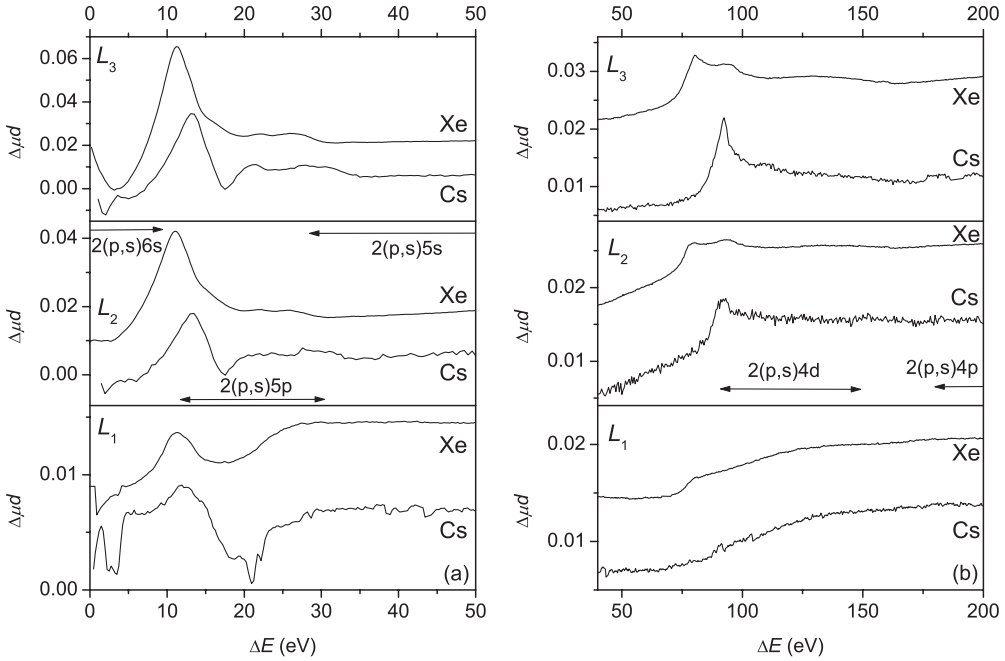

FIG. 6. MPE on the relative energy scale with arbitrary background up to quadratic terms in E removed to expose the sharp features.

relatively weak $1s3d$ excitation in Rb and Kr [1]. L spectra of Cs and Xe provide much more definite evidence.

The $2s4d$ feature in Cs and Xe is sufficiently well isolated that the shake probability can be reliably estimated: The result $5\% \pm 1\%$ of the probability for single ionization is close to the theoretical result 5.6% of Carlson and Nestor [28] and to the value of 6% for the corresponding shake feature in the K-edge absorption [3].

IV. CONCLUSIONS

The atomic absorption of Cs provides, in combination with much studied Xe absorption, some insight into systematic effects in the L-shell photoeffect. The composition of the edge profiles and the sequence of the MPE fingerprints have much in common in both elements. Generally, Cs shows sharper and richer structure: The same has been found in other alkali-metal–noble-gas pairs K-Ar [2] and Rb-Kr [1]. The MPE in the L_1 region can be understood by the application of approaches and principles established in the study of the K-edge domain. The L_2 and L_3 edge regions, at first sight appearing to be identical copies except for a factor of 2, follow smooth baselines of specific shapes, recently well reconstructed in Xe by an advanced RRPARC calculation.

In addition, the analysis of the edge profiles and the identification of the sharp MPE features present novel material for testing theoretical models and for the construction of the atomic absorption background for extended x-ray absorption fine structure analysis involving nearby elements.

ACKNOWLEDGMENTS

This work was supported by the Slovenian Research Agency research program P1-0021 and by DESY and the European Community's Seventh Framework Programme (FP7/2007–2013) ELISA (European Light Sources Activities) under Grant No. 226716. Access to synchrotron radiation facilities of HASYLAB (Project No. II-20080058 EC) and ELETTRA is acknowledged. We would like to thank Edmund Welter of HASYLAB and L. Olivi of ELETTRA Sincrotrone Trieste for expert advice on beamline operation.

[1] A. Kodre, I. Arcon, J. Padeznik Gomilsek, R. Preseren, and R. Frahm, J. Phys. B **35**, 3497 (2002).
[2] J. P. Gomilsek, A. Kodre, I. Arcon, and R. Preseren, Phys. Rev. A **64**, 022508 (2001).
[3] J. P. Gomilsek, A. Kodre, I. Arcon, and M. Hribar, Phys. Rev. A **68**, 042505 (2003).
[4] A. Mihelic, A. Kodre, I. Arcon, J. Padeznik Gomilsek, and M. Borowski, Nucl. Instrum. Methods Phys. Res. B **196**, 194 (2002).
[5] A. Kodre, J. Padeznik Gomilsek, A. Mihelic, and I. Arcon, Rad. Phys. Chem. **75**, 188 (2006).
[6] U. Arp, B. M. Lagutin, G. Materlik, I. D. Petrov, B. Sonntag, and V. L. Sukhorukov, J. Phys. B **26**, 4381 (1993).
[7] J. P. Gomilsek, I. Arcon, S. de Panfilis, and A. Kodre, Phys. Rev. A **79**, 032514 (2009).
[8] K. Zhang, E. A. Stern, J. J. Rehr, and F. Ellis, Phys. Rev. B **44**, 2030 (1991).
[9] I. Arcon, A. Kodre, M. Stuhec, D. Glavic-Cindro, and W. Drube, Phys. Rev. A **51**, 147 (1995).
[10] A. Filipponi, L. Ottaviano, and T. A. Tyson, Phys. Rev. A **48**, 2098 (1993).

[11] J. Padeznik Gomilsek, A. Kodre, I. Arcon, and V. Nemanic, Nucl. Instrum. Methods Phys. Res. B **266**, 677 (2008).
[12] R. D. Deslattes *et al.*, *X-ray Transition Energies* (version 1.2) (National Institute of Standards and Technology, Gaithersburg, MD, 2005), [http://physics.nist.gov/XrayTrans].
[13] A. Di Cicco, G. Aquilanti, M. Minicucci, E. Principi, N. Novello, A. Cognigni, and L. Olivi, J. Phys. Conf. Ser. **190**, 012043 (2009).
[14] A. Filipponi, J. Phys. B **33**, 2835 (2000).
[15] M. Breinig, M. H. Chen, G. E. Ice, F. Parente, B. Crasemann, and G. S. Brown, Phys. Rev. A **22**, 520 (1980).
[16] C. M. Teodorescu, R. C. Karnatak, J. M. Esteva, A. El Afif, and J.-P. Connerade, J. Phys. B **26**, 4019 (1993).
[17] J. Tulkki and T. Aberg, J. Phys. B **18**, L489 (1985).
[18] M. Y. Amusia, V. K. Ivanov, and V. A. Kupchenko, J. Phys. B **14**, L667 (1981).
[19] C. Froese-Fischer, Comput. Phys. Commun. **43**, 355 (1987).
[20] M. A. Amusia, A. S. Baltenkov, and G. I. Zhuravleva, J. Phys. B **29**, L151 (1996).
[21] W. Jitschin and R. Stotzel, Phys. Rev. A **58**, 1221 (1998).
[22] M. Kutzner, Rad. Phys. Chem. **70**, 95 (2004).
[23] M. J. Berger, J. H. Hubbell, S. M. Seltzer, J. Chang, J. S. Coursey, R. Sukumar, and D. S. Zucker, *XCOM: Photon Cross Section Database* (version 1.3) (National Institute of Standards and Technology, Gaithersburg, MD, 2005), [http://physics.nist.gov/xcom].
[24] K. G. Dyall, I. P. Grant, C. T. Johnson, F. A. Parpia, and E. P. Plummer, Comput. Phys. Commun. **55**, 425 (1989).
[25] I. Arcon, A. Kodre, J. Padeznik Gomilsek, M. Hribar, and A. Mihelic, Phys. Scr. T **115**, 235 (2005).
[26] J. A. Solera, J. Garcia, and M. G. Proietti, Phys. Rev. B **51**, 2678 (1995).
[27] A. Kodre, I. Arcon, M. Hribar, M. Stuhec, F. Villain, and P. Parent, J. Phys. (Paris) C **9**, 397 (1994).
[28] T. A. Carlson and C. W. Nestor, Phys. Rev. A **8**, 2887 (1973).